Supplementary materials

The Dolabellane Diterpenes as Potential Inhibitors of SARS-CoV-2 Main Protease: Molecular Insight of Inhibitory Mechanism through Computational Studies

Nanik Siti Aminah[a,b*], Muhammad Ikhlas Abdjan[a,c], Andika Pramudya Wardana[a,c], Alfinda Novi Kristanti[a,b], Imam Siswanto[a,d], Khusna Arif Rakhman[e], Yoshiaki Takaya[f]

[a] Departement of Chemistry, Faculty of Science and Technology, Universitas Airlangga, Surabaya 60115, Indonesia. E-mail: nanik-s-a@fst.unair.ac.id

[b] Biotechnology of Tropical Medicinal Plants Research Group, Universitas Airlangga

[c] Ph.D. Student of Mathematics and Natural Sciences, Faculty of Science and Technology, Universitas Airlangga, Komplek Kampus C UNAIR, Jl. Mulyorejo, 60115, Surabaya, Indonesia

[d] Bioinformatic Laboratory, UCoE Research Center for Bio-Molecule Engineering Universitas Airlangga, Surabaya, Indonesia

[e] Departement of Chemistry Education, Universitas Khairun, Ternate,

[f] Faculty of Pharmacy, Meijo University, Nagoya, Japan

Table S1 Molecular Docking Results: Energy Components (kcal/mol) of the Inhibitor-3CL^{pro}

Code	Grid Score	E_{vdW}	E_{ele}
0EN-3CL^{pro}	-72.58	-66.28	-6.30
DD1-3CL^{pro}	-41.39	-40.00	-1.39
DD2-3CL^{pro}	-41.20	-41.33	0.13
DD3-3CL^{pro}	-47.71	-47.43	-0.28
DD4-3CL^{pro}	-37.81	-35.55	-2.25
DD5-3CL^{pro}	-42.93	-41.86	-1.07
DD6-3CL^{pro}	-48.50	-46.69	-1.80
DD7-3CL^{pro}	-45.74	-45.84	0.09
DD8-3CL^{pro}	-47.62	-47.09	-0.53
DD9-3CL^{pro}	-72.66	-72.09	-0.57
DD10-3CL^{pro}	-67.95	-69.34	1.39
DD11-3CL^{pro}	-68.58	-67.34	-1.24
DD12-3CL^{pro}	-65.67	-64.32	-1.35
DD13-3CL^{pro}	-74.53	-70.60	-3.93
DD14-3CL^{pro}	-65.68	-65.58	-0.09

Table S2 The average value of trajectories during the simulation time. Data are shown as mean ± standard deviation (SD).

Parameters	$3CL^{pro}$	$0EN\text{-}3CL^{pro}$	$DD9\text{-}3CL^{pro}$	$DD13\text{-}3CL^{pro}$
100 ns				
Total Energy (kcal/mol)	-111568 ± 984.48	-111413 ± 976.49	-110988 ± 984.74	-111077 ± 987.73
RMSD-Complex (nm)	0.25 ± 0.04	0.26 ± 0.04	0.26 ± 0.04	0.27 ± 0.04
RMSD-Backbone (nm)	0.19 ± 0.04	0.20 ± 0.05	0.18 ± 0.03	0.20 ± 0.05
RMSD-Ligand (nm)	-	0.16 ± 0.03	0.24 ± 0.03	0.22 ± 0.03
Last 20 ns				
RMSF (nm)	0.32 ± 0.10	0.45 ± 0.15	0.39 ± 0.13	0.53 ± 0.20
B-Factor (nm^2)	3.09 ± 1.85	5.92 ± 3.61	4.51 ± 2.90	8.65 ± 5.84
RoG (nm)	2.23 ± 0.01	2.20 ± 0.00	2.22 ± 0.01	2.23 ± 0.01
SASA-All Surface(nm^2)	146.32 ± 2.62	142.08 ± 2.54	147.45 ± 3.14	143.73 ± 2.84
SASA-Active Site (nm^2)	10.85 ± 0.78	9.98 ± 0.79	16.20 ± 0.82	11.61 ± 0.62
Atom Contacts	-	8.00 ± 2.00	2.00 ± 1.00	8.00 ± 2.00

Table S3 Atom contacts detail of the inhibitor-3CL^{pro}: The percentage of atom contacts (P_{AC}) and distance average (Avg).

No	Contact	Frames	Fraction	Avg (Å)	P_{AC} (%)
0EN-3CL^{pro}					
1	N3…NE2(HIE163)	1978	0.99	3.04	98.90
2	O2…N(GLU166)	1944	0.97	2.91	97.20
3	O1…N(GLY143)	1873	0.94	3.04	93.65
4	C21…O(LEU141)	1698	0.85	3.19	84.90
5	O1…CA(ASN142)	1581	0.79	3.28	79.05
6	O1…ND2(ASN142)	1261	0.63	2.99	63.05
7	N3…CE1(HIE163)	1018	0.51	3.34	50.90
8	C20…O(LEU141)	971	0.49	3.31	48.55
9	O1…CB(ASN142)	938	0.47	3.32	46.90
10	C20…C(LEU141)	881	0.44	3.36	44.05
11	C19...ND2(ASN142)	611	0.31	3.33	30.55
12	C20…OE1(GLU166)	366	0.18	3.33	18.30
13	C21…C(LEU141)	353	0.18	3.40	17.65
14	C20…N(ASN142)	332	0.17	3.39	16.60
15	O1…CG(ASN142)	324	0.16	3.38	16.20
16	C20…CD(GLU166)	23	0.01	3.43	1.15
DD9-3CL^{pro}					
1	O30…N(THR26)	1921	0.96	3.00	96.05
2	O30…CA(THR25)	1163	0.58	3.34	58.15
3	O30…O(THR26)	872	0.44	3.31	43.60
4	C49…C(THR45)	485	0.24	3.39	24.25
5	O30…C(THR25)	238	0.12	3.44	11.90
6	C52…O(THR24)	167	0.08	3.36	8.35
7	C44…CA(THR45)	41	0.02	3.43	2.05
8	C45…CB(THR45)	16	0.01	3.44	0.80
9	C24…ND2(ASN142)	3	0.00	3.37	0.15
DD13-3CL^{pro}					
1	O30…NE2(GLN189)	1977	0.99	2.94	98.85
2	O15…CD2 (HIE41)	1915	0.96	3.14	95.75
3	N59…OG(SER144)	1877	0.94	3.10	93.85
4	N59…NE2(HIE163)	1849	0.92	3.09	92.45
5	O25…ND2(ASN142)	1387	0.69	3.00	69.35
6	O54…O(HIE164)	785	0.39	3.28	39.25
7	N59…O(LEU141)	725	0.36	3.31	36.25
8	C60…NE2(HIE163)	678	0.34	3.39	33.90
9	C44…O(GLN189)	642	0.32	3.30	32.10
10	O15…CG(GLN189)	633	0.32	3.36	31.65
11	C58…O(LEU141)	569	0.28	3.32	28.45
12	C14…CG(GLN189)	510	0.26	3.42	25.50
13	C53…O(HIE164)	491	0.25	3.32	24.55
14	O25…OD1(ASN142)	346	0.17	3.31	17.30
15	C49…O(GLU166)	337	0.17	3.34	16.85
16	O25…CG(ASN142)	312	0.16	3.34	15.60
17	C31…O(CYS44)	218	0.11	3.38	10.90
18	C31…CG2(THR25)	196	0.10	3.41	9.80
19	C37…SD(MET49)	26	0.01	3.41	1.30
20	C58…NE2(HIE163)	5	0.00	3.47	0.25

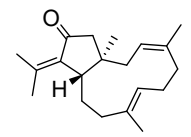

DD1

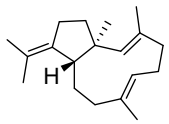

DD2

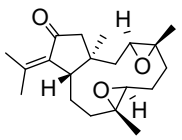

DD3

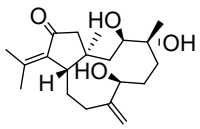

DD4

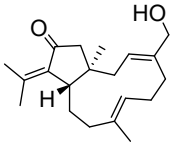

DD5

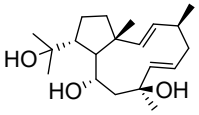

DD6

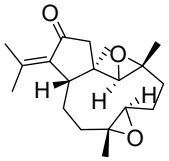

DD7

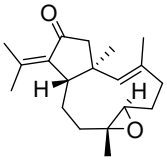

DD8

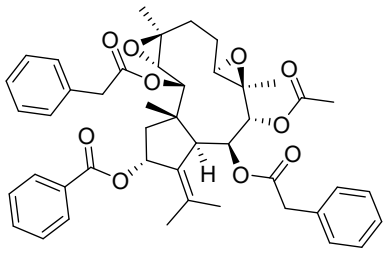

DD9

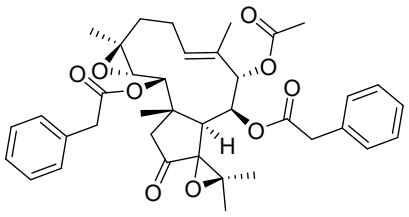

DD10

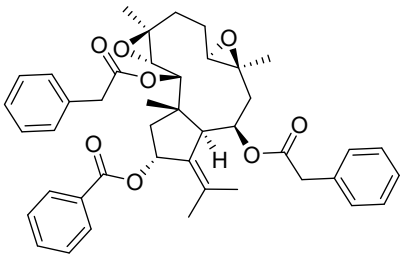

DD11

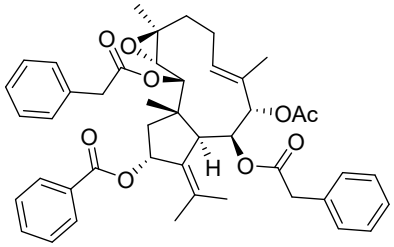

DD12

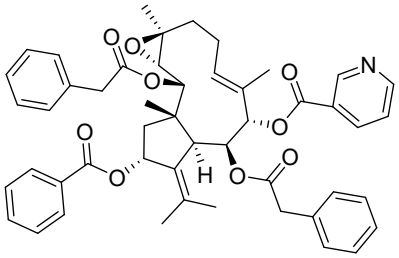

DD13

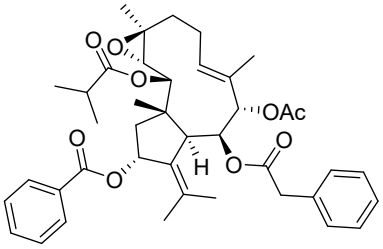

DD14

Fig. S1 Dolabellane diterpene as candidate

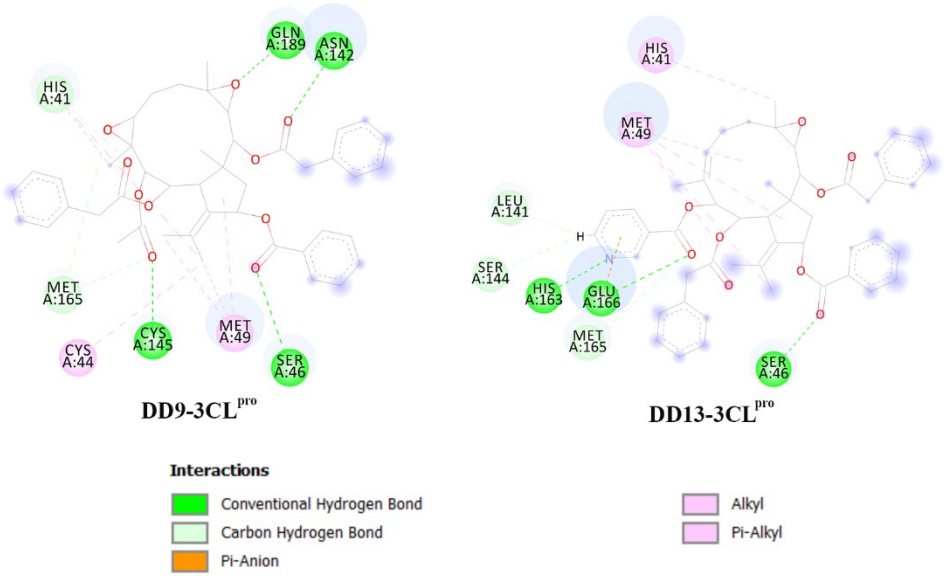

Fig. S2 Selected candidates based on lower grid-score: The interaction types of inhibitor-3CL^{pro} shows in the 2D diagram.

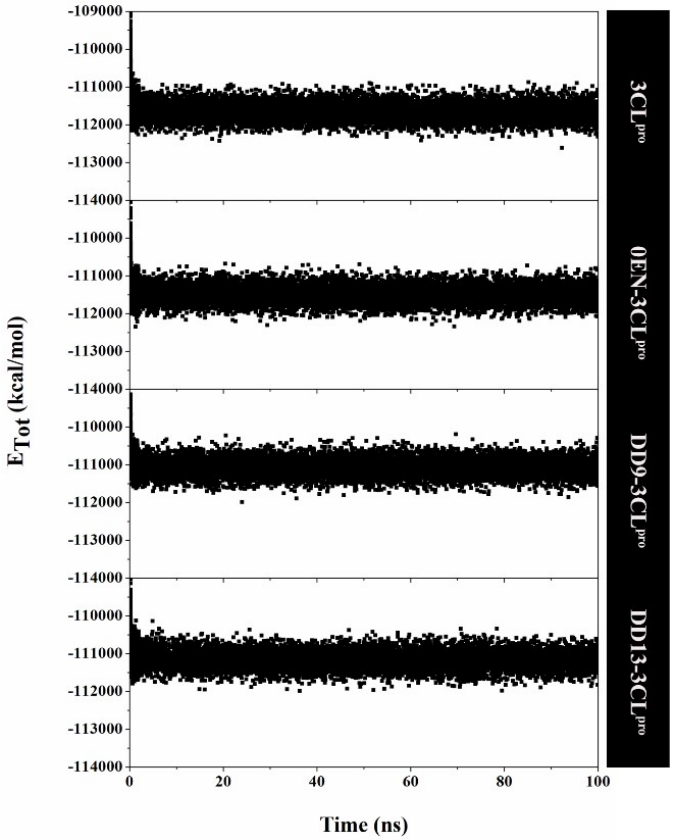

Fig. S3 The total energy was plotted along 100 ns of MD simulation of each system using the *mdout* analysis.

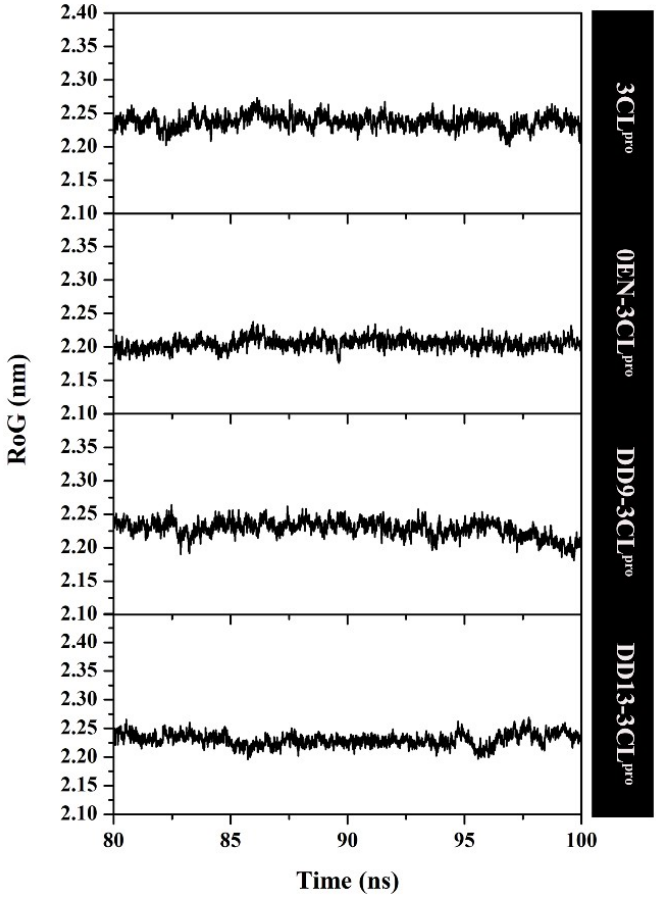

Fig. S4 The radius of gyration of each system was plotted along the last 20 ns of MD simulation.

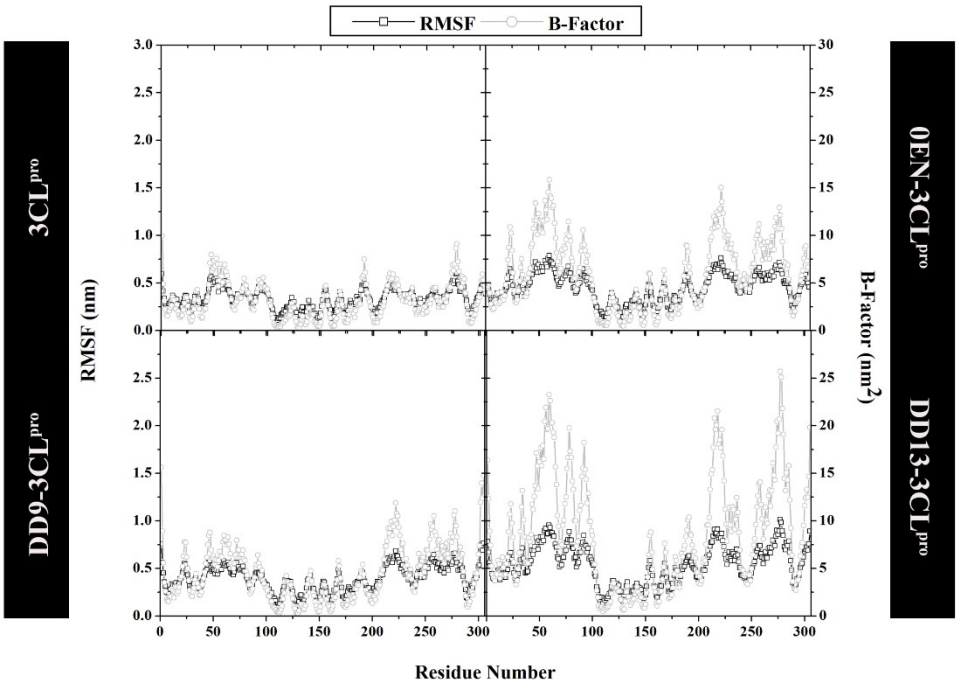

Fig. S5 Flexibility Analysis: The root-mean-square fluctuation and B-factor plotted along the last 20 ns of MD simulation.

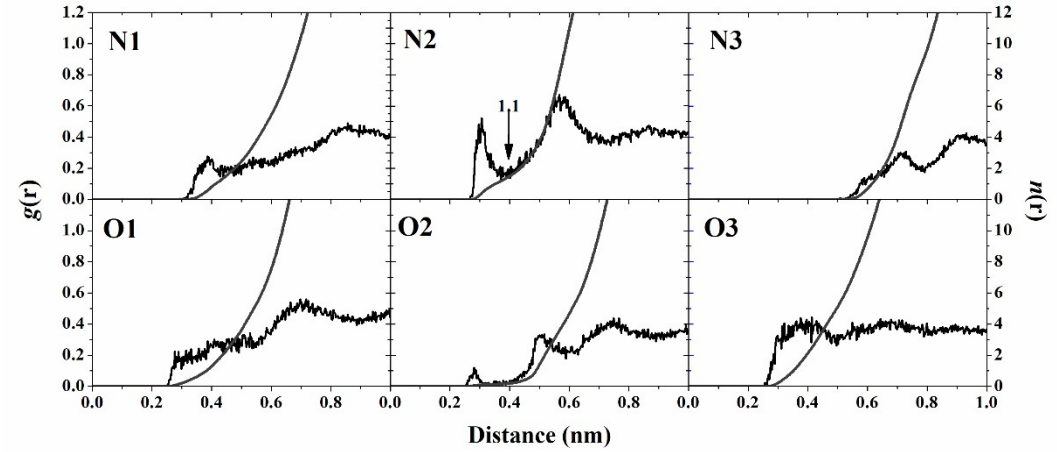

Fig. S6 The radial distribution functions (*g*(r)) of the water oxygen atom and integration numbers (*n*(r)), up to the first minimum around the heteroatoms (black arrow) of 0EN-3CL^{pro} during the simulation over the last 20 ns.

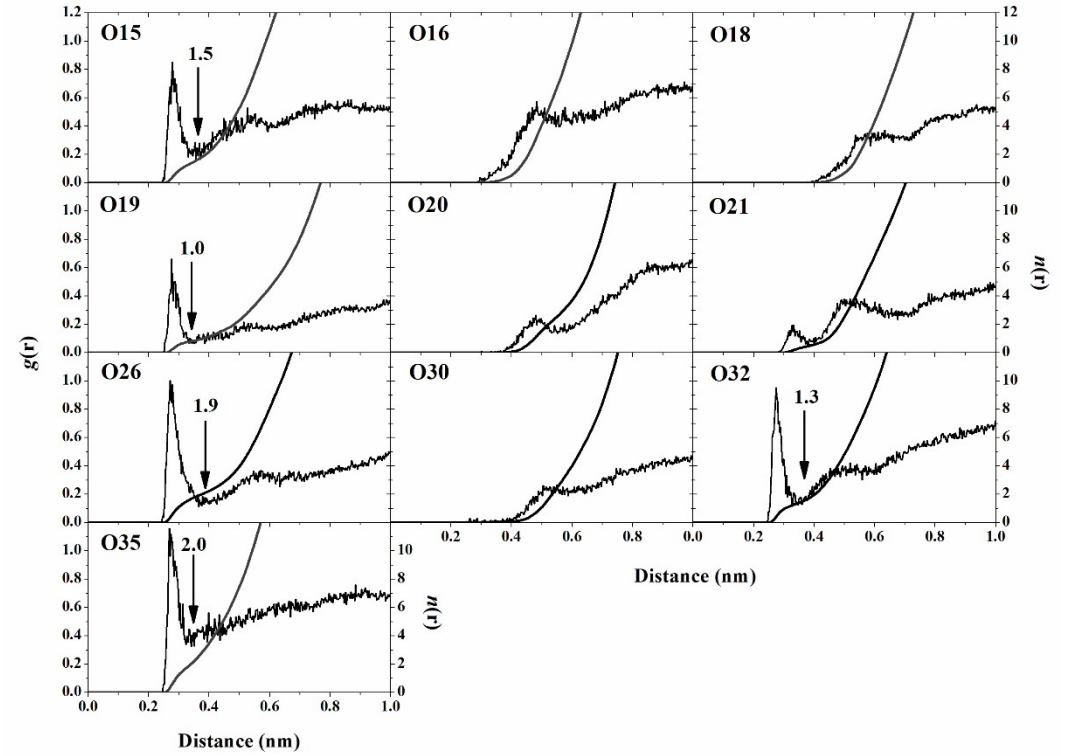

Fig. S7 The radial distribution functions (*g*(r)) of the water oxygen atom and integration numbers (*n*(r)), up to the first minimum around the heteroatoms (black arrow) of DD9-3CL^{pro} during the simulation over the last 20 ns.

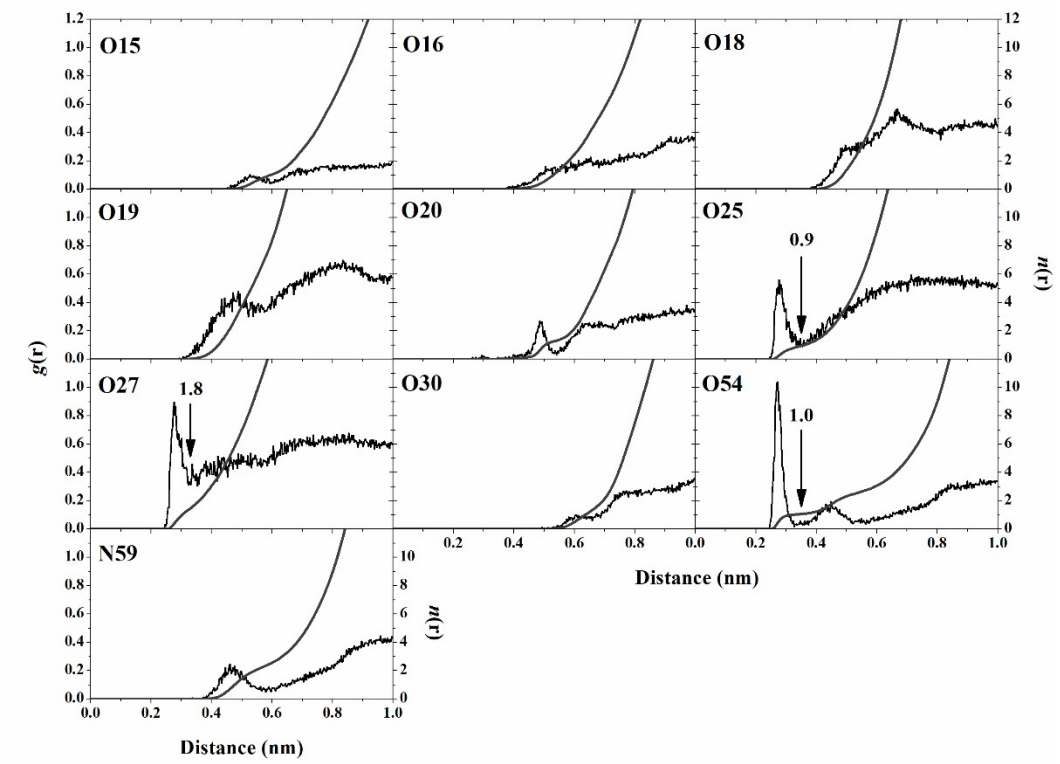

Fig. S8 The radial distribution functions (*g*(r)) of the water oxygen atom and integration numbers (*n*(r)), up to the first minimum around the heteroatoms (black arrow) of DD13-3CL^{pro} during the simulation over the last 20 ns.

Residues	Subsite	0EN-3CL^{pro}	DD9-3CL^{pro}	DD13-3CL^{pro}
THR25	S2'	-0.20	-2.54	-1.01
THR26	S2'	-0.13	-1.62	-0.22
LEU27	S2'	-0.63	-1.02	-0.92
HIE41	S2	-1.33	-1.38	-2.68
CYS44	S2	-0.16	-1.08	-1.09
THR45	S2	-0.04	-1.35	-0.87
SER46	S2	-0.06	-1.73	-1.36
MET49	S2	-1.89	-3.13	-3.09
TYR54	S2	-0.66	-0.07	-0.13
LEU141	S1	-0.89	-0.14	-0.83
ASN142	S1	-2.08	-1.43	-2.85
GLY143	S1	-0.88	-1.01	-0.39
SER144	S1	-0.66	-0.12	-0.58
CYS145	S1	-1.41	-0.18	-1.42
HIE163	S1	-0.34	-0.03	-0.55
HIE164	S2	-0.81	-0.04	-1.60
MET165	S2	-2.76	-0.03	-2.77
GLU166	S3	-2.24	-0.04	-2.50
LEU167	S4	-0.25	-0.01	-0.32
HIE172	S1	-0.79	-0.01	-0.44
ASP187	S2	-0.79	0.00	-0.33
ARG188	S2	-0.67	-0.01	-0.56
GLN189	S4	-1.07	-0.05	-3.31

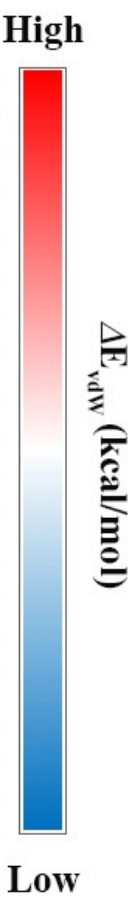

Fig. S9 The van der Waals contact of each complex in the 3CL^{pro} subsite binding pocket plotted along 20 ns last trajectories.